

Article

# Degradation and Loss of Antibacterial Activity of Commercial Amoxicillin with TiO<sub>2</sub>/WO<sub>3</sub>-Assisted Solar Photocatalysis

Augusto Arce-Sarria <sup>1</sup>, Fiderman Machuca-Martínez <sup>1</sup> , Ciro Bustillo-Lecompte <sup>2</sup> ,  
Aracely Hernández-Ramírez <sup>3</sup> and José Colina-Márquez <sup>4,\*</sup> 

<sup>1</sup> Escuela de Ingeniería Química, Universidad del Valle, Cali A.A. 25360, Colombia; augusto.arce@correounivalle.edu.co (A.A.-S.); fiderman.machuca@correounivalle.edu.co (F.M.-M.)

<sup>2</sup> School of Occupational and Public Health, Ryerson University, 350 Victoria Street, Toronto, ON M5B 2K3, Canada; ciro.lecompte@ryerson.ca

<sup>3</sup> Facultad de Ciencias Químicas, Universidad de Nuevo León, CP 64570 Monterrey, Nuevo Leon, Mexico; aracely.hernandezrm@uanl.edu.mx

<sup>4</sup> Chemical Engineering Program, Universidad de Cartagena, Av. El Consulado 48-152, Cartagena A.A. 130001, Colombia

\* Correspondence: jcolinam@unicartagena.edu.co; Tel.: +57-311-788-1188

Received: 30 April 2018; Accepted: 21 May 2018; Published: 23 May 2018



**Abstract:** In this study, a TiO<sub>2</sub> catalyst, modified with tungsten oxide (WO<sub>3</sub>), was synthesized to reduce its bandgap energy (E<sub>g</sub>) and to improve its photocatalytic performance. For the catalyst evaluation, the effect of the calcination temperature on the solar photocatalytic degradation was analyzed. The experimental runs were carried out in a CPC (compound parabolic collector) pilot-scale solar reactor, following a multilevel factorial experimental design, which allowed analysis of the effect of the calcination temperature, the initial concentration of amoxicillin, and the catalyst load on the amoxicillin removal. The most favorable calcination temperature for the catalyst performance, concerning the removal of amoxicillin, was 700 °C; because it was the only sample that showed the rutile phase in its crystalline structure. Regarding the loss of the antibiotic activity, the inhibition tests showed that the treated solution of amoxicillin exhibited lower antibacterial activity. The highest amoxicillin removal achieved in these experiments was 64.4% with 100 ppm of amoxicillin concentration, 700 °C of calcination temperature, and 0.1 g L<sup>-1</sup> of catalyst load. Nonetheless, the modified TiO<sub>2</sub>/WO<sub>3</sub> underperformed compared to the commercial TiO<sub>2</sub> P25, due to its low specific surface and the particles sintering during the sol-gel synthesis.

**Keywords:** sol-gel; bandgap energy; CPC; emergent pollutants; photodegradation

## 1. Introduction

Heterogeneous photocatalysis, based on TiO<sub>2</sub>, has been widely used for environmental applications such as removal of contaminants and water disinfection due to its oxidative reactions [1–3]. However, TiO<sub>2</sub> shows a significant limitation when solar radiation is used for promoting the formation of oxidant species including hydroxyl radicals (•OH) because TiO<sub>2</sub> uses only a small fraction of the electromagnetic spectrum corresponding to the UV (Ultraviolet) radiation (wavelengths shorter than 400 nm) [4,5]. To improve the usage of the solar spectrum, several alternatives have been proposed, including catalyst doping, dye-sensitization, and modification with other oxides [6,7].

Ramos-Delgado et al. [8,9] observed the highest photocatalytic activity of TiO<sub>2</sub>/WO<sub>3</sub> materials while using 1% w/w of WO<sub>3</sub>. Thus, the selection of WO<sub>3</sub> as modifying oxide is encouraged by the

reduction of the bandgap energy ( $E_g = 2.8$  eV), which has also been reported for  $\text{TiO}_2$  in a previous work [10].

The reduction of the  $E_g$  improves the radiation usage by the photocatalyst since  $\text{WO}_3$  can act as an electron-accepting species and reduces the recombination rate of the electron-hole pairs. Regarding the photocatalytic mechanism, the semiconductor  $\text{TiO}_2$  is responsible for the electron exchange in the redox reactions and  $\text{WO}_3$  can act as a defect of the crystalline structure, inserting an energetic localized state [8,9].

For assessing the photocatalytic activity of the  $\text{TiO}_2/\text{WO}_3$  material, the oxidation of a commercial antibiotic (amoxicillin) was studied in the presence of solar radiation. Amoxicillin is one of the most consumed antibiotics worldwide and concentrations in the range of  $3\text{--}87 \mu\text{g L}^{-1}$  have been reported for hospital effluents [11]. In general, antibiotics have been classified as emergent pollutants due to the potential risks involved with their presence in water bodies and the recent interest in looking for treatment alternatives for their removal. The highest environmental risk of these drugs is the development of waterborne pathogens resistant to the antibiotic activity. Therefore, their natural resistance to biological wastewater treatments has directed the research to novel and more effective technologies for removing these pollutants [12].

Amoxicillin is recognized to be highly refractory and persistent in aquatic ecosystems. Due to the non-selective nature of  $\bullet\text{OH}$ , several emergent contaminants, including amoxicillin, can be entirely oxidized by advanced oxidation processes (AOPs) as previously reported [13–15]. Photo-Fenton has been reported as an alternative for amoxicillin removal, achieving 52% of total organic carbon (TOC) reduction [16]. Regarding heterogeneous photocatalysis, few applications with  $\text{TiO}_2/\text{WO}_3$  as a catalyst have been reported. Ramos-Delgado et al. [8] synthesized  $\text{TiO}_2$  modified with  $\text{WO}_3$  for degrading Malathion, an organophosphorus pesticide. The TOC removal in this work was 78%, comparable with the 47% removal obtained with bare  $\text{TiO}_2$ . It is important to note that for  $\text{TiO}_2/\text{WO}_3$ , there are no reports of antibiotics removal. However, there are previous studies of  $\text{TiO}_2$  doped with Fe and C where 78% of amoxicillin removal was achieved [12,17], evidencing the satisfactory performance of the photocatalysis for eliminating amoxicillin.

This work assessed the photocatalytic activity, not only based on the amoxicillin degradation or the TOC removal but also estimating the loss of the antibacterial activity. It has been found that despite achieving a complete degradation of amoxicillin, even with high TOC removals, the presence of the remaining intermediates can show some antibacterial activity [18]. Regarding bacterial inactivation, this can be more harmful than the presence of the parent antibiotic since waterborne bacteria may develop a more effective resistance to antibiotic activity. Nevertheless, there is no information about the survival or regrowth rates for specific bacteria in such conditions.

Regarding the use of solar radiation as photon source, this is precisely one of the advantages of the reduction of the  $E_g$  for the  $\text{TiO}_2/\text{WO}_3$ -based photocatalysis [9,19,20]. It is expected to observe a better performance of the modified  $\text{TiO}_2$  in comparison with bare  $\text{TiO}_2$  due to a broader absorption of the radiation spectrum of the modified photocatalyst, as mentioned earlier. The experiments of this research were carried out in a pilot-scale CPC photoreactor [21] under the tropical weather conditions of Cali, Colombia, to evaluate the activity of the modified  $\text{TiO}_2$  with solar radiation for removing commercial amoxicillin. Moreover, the kinetics was studied by fitting the parameters of a modified Langmuir-Hinshelwood expression with experimental data gathered from the solar photocatalytic tests. The accumulated UV energy was chosen as the independent variable instead of time in this kinetic analysis, because of the variation of the solar irradiation during the experimental runs. This approach allows a consideration of a more accurate manner of a potential scale-up of the photoreactor since the photocatalytic reaction rate depends on the photon absorption as it has been reported in previous studies [22,23].

## 2. Results

### 2.1. Effect of the Calcination Temperature on the TiO<sub>2</sub>/WO<sub>3</sub> Characterization

The Kubelka-Munk theory was applied to obtain the  $E_g$  and hence the absorption wavelength of the material [19–21,24–26]. Figure 1 shows that the lowest reflectance (highest UV absorbance) was observed for the sample calcined at 500 °C. Ramos-Delgado et al. [8] synthesized TiO<sub>2</sub>/WO<sub>3</sub> (2% w/w) using the same calcination temperature, obtaining satisfactory results in terms of the particle size and the  $E_g$ . Although it was expected to obtain higher reflectance values at higher temperatures, the performance with a calcination temperature of 700 °C shows an intermediate reflectance. As reported in other studies [27,28], this can be related to the ratio of anatase/rutile present in the synthesized material. The calcination temperature can affect the formation of determined crystalline phase and the ratio of these phases [29]. Although it is reported that rutile is the most photoactive phase, it is also the most unstable. The rutile phase appears at temperatures higher than 600 °C; therefore, the lower transmittance observed at 700 °C can be attributed to this phenomenon.

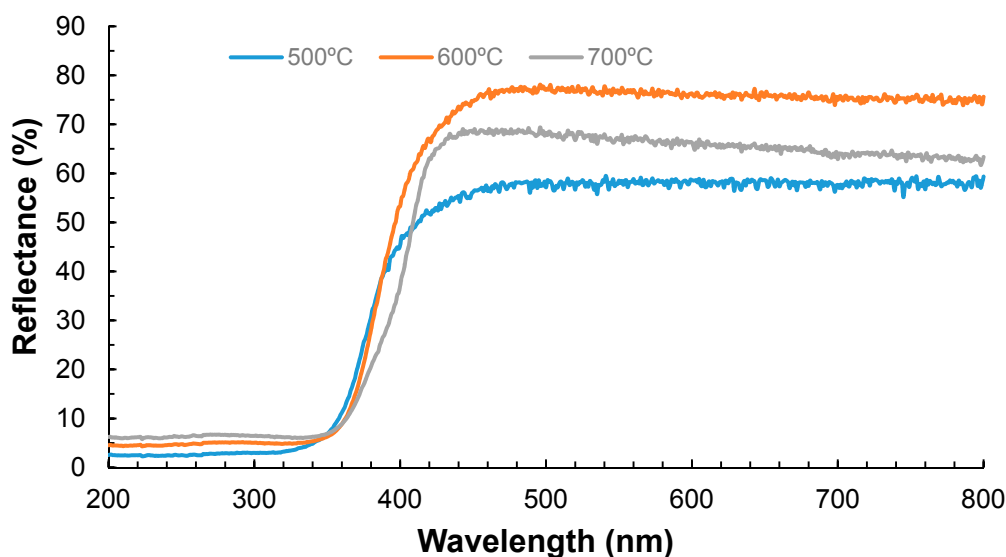


**Figure 1.** DRS (diffuse reflectance spectroscopy)-UV Vis spectra for 1% TiO<sub>2</sub>/WO<sub>3</sub> at different temperatures.

The Kubelka-Munk function (Equation (1)) was used for estimating the  $E_g$  based on the reflectance values obtained in Figure 1 for each synthesized material, as follows [30]:

$$F(R_\infty) = \frac{(1 - R_\infty)^2}{2R_\infty} \quad (1)$$

where  $R_\infty$  corresponds to the ratio between the sample reflectance and a blank reflectance measured in the same equipment. These values are not shown in the manuscript due to the high amount of data obtained from the DRS analysis. The  $E_g$  could be calculated with the following equation:

$$[F(R_\infty)hv]^{0.5} = C_2(hv - E_g) \quad (2)$$

The plot of  $[F(R_\infty)hv]^{0.5}$  vs.  $hv$  (Figure 2) allowed to estimate the  $E_g$  based on the intercept of the tangent of the obtained curve. For the case of the sample calcined at 700 °C, the obtained value of  $E_g$  was 2.84 eV. The  $E_g$  results and the maximal wavelength of absorbed radiation for the samples calcined at different temperatures are shown in Table 1.

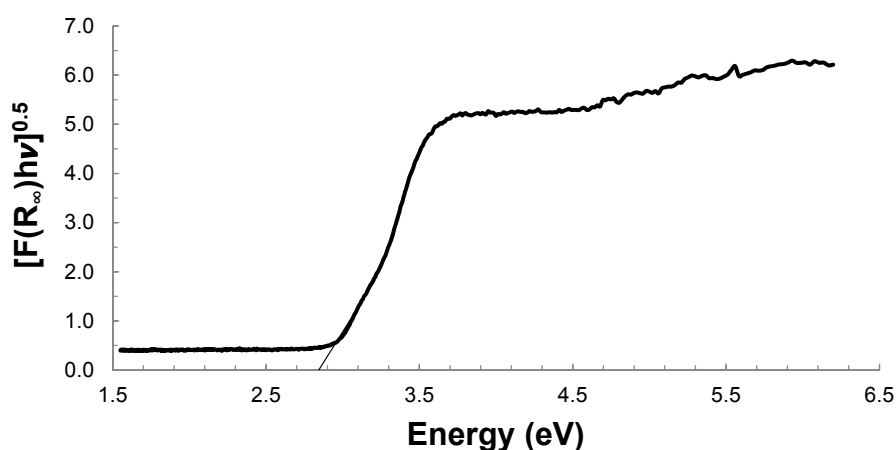


**Figure 2.**  $E_g$  determination for photocatalyst calcined at 700 °C.

**Table 1.** Bandgap energy and maximum wavelength of radiation absorption.

	Calcination Temperature		
	500 °C	600 °C	700 °C
$E_g$ (eV)	3.12	3.12	2.84
$\lambda$ (nm)	397	397	436

The reduction of the  $E_g$  with respect to bare  $\text{TiO}_2$  (3.2 eV) is related to the modification of its crystalline structure due to insertion of the  $\text{WO}_3$ . The function of this oxide is to add a localized state into the energy gap between the conduction and the valence bands. Furthermore, the insertion of the  $\text{WO}_3$  (an electron acceptor species) increases the density of energy holes or vacancies on the  $\text{TiO}_2$  surface, and this prevents the electron-hole recombination [8]. As seen in Table 1, the best  $E_g$  was obtained at 700 °C, and this result is consistent with the one observed in Figure 1. The  $E_g$  values for 500 and 600 °C were the same, but slightly lower than the corresponding one to bare  $\text{TiO}_2$ . Higher calcination temperatures can promote the formation of the rutile crystalline phase, which has a lower  $E_g$  than the anatase phase. However, these changes could not be detected by XRD (X-ray Diffraction) (Figure 3) due to the low concentrations of the  $\text{WO}_3$ .

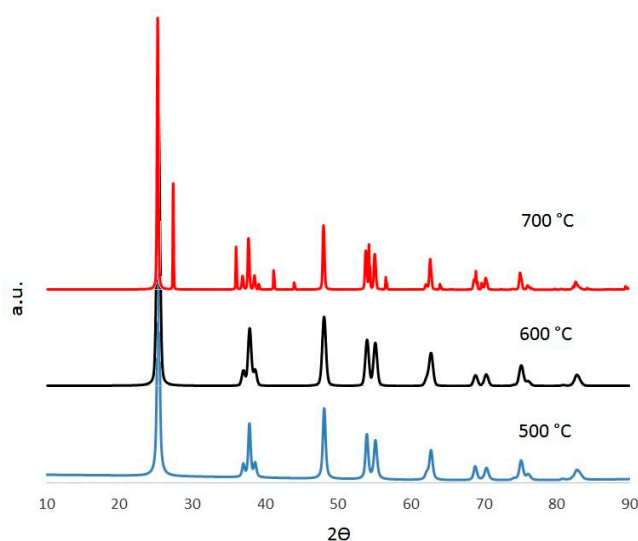


**Figure 3.** XRD for different synthesized materials.

The difference between the bandgap energies obtained at higher calcination temperatures can be attributed to the characteristic retention of the OH groups by the solids prepared by the sol-gel method [8]. Because of the  $E_g$  reduction, compared to bare  $\text{TiO}_2$ ,  $\text{TiO}_2/\text{WO}_3$  can absorb radiation under 465 nm of wavelength, which means that the material can use part of the visible spectrum of light, as reported in previous works [9,19,20,23,31,32].

Figure 3 shows the XRD patterns obtained with the three different calcination temperatures. There is only one crystalline phase at 500 and 600 °C corresponding to the anatase (tetragonal) structure [8]; whereas, at 700 °C two phases appear, corresponding to a mixture of anatase (JCPDS 98-009-6394) and rutile (JCPDS 98-004-1028) structures [33]. This result is consistent with those shown in Figure 1, where the DRS obtained at 700 °C showed a lower reflectance than the one obtained at 600 °C. This outcome is congruent with the reported literature [8–10] since the rutile phase has a lower  $E_g$  than the anatase phase, as mentioned previously. Regarding  $\text{WO}_3$ , its presence could not be detected by XRD because of its low content in the photocatalyst [10].

The values of the crystal diameter (perpendicular and parallel) and the proportions of the phases were obtained by processing the data with the X'Pert (Malvern Panalytical, Malvern, United Kingdom), GSAS (Edgewall Software, Pittsburgh, PN, USA), and EXPGUI (Edgewall Software, Pittsburgh, PN, USA) software packages, as seen in Table 2.

**Table 2.** Crystal diameters.

	500 °C	600 °C	700 °C	
	Anatase	Anatase	Anatase	Rutile
$\varnothing_{\text{perp}}$ (nm)	59	58	116	820
$\varnothing_{\text{para}}$ (nm)	83	37	137	204

It is important to note that the sample calcined at 700 °C exhibited an anatase/rutile ratio: 74/26; nonetheless, the average crystal diameters are much larger than the obtained ones at 500 and 600 °C. The large crystal sizes are the product of the clustering of the  $\text{WO}_3$  on the  $\text{TiO}_2$  surface as reported in similar studies [8,9]. Although the presence of these clusters can be beneficial for the photocatalytic activity since they can avoid the hole-electron recombination, a larger crystal may affect the performance of the material in photocatalytic reactions negatively, because of the significant decrease of the surface area.

The results in Table 3 are the logical consequence of the behavior observed in Table 2. As the crystal size increases, the surface area decreases as expected. The significant reduction of the surface area for the sample calcined at 700 °C may be related to the formation of  $\text{WO}_3$  clusters mentioned previously.

**Table 3.** Surface area and average pore diameter.

Calcination Temperature (°C)	Surface Area ( $\text{m}^2 \text{g}^{-1}$ )	Average Pore Diameter (nm)
500	66.45	77.53
600	35.93	77.31
700	4.970	122.40

Regarding the pore diameter, the results for the catalysts calcined at the different temperatures show similar diameters for the samples obtained at 500 and 600 °C (~77 nm); however, a much larger diameter (122.40 nm) was exhibited for the 700 °C sample. This last result represents a potential positive effect for the photocatalytic reaction because the mass transport through the catalyst pore will be easier than in smaller pores. The decrease of the surface area, with the subsequent increase of the pore size, can be explained due to the material sintering during the calcination at higher temperatures.

From the obtained results after carrying out physical adsorption tests with nitrogen, it can be said that the solids are considered as mesoporous. This outcome was confirmed by the presence of hysteresis in the adsorption and desorption processes, as seen in Figure 4.

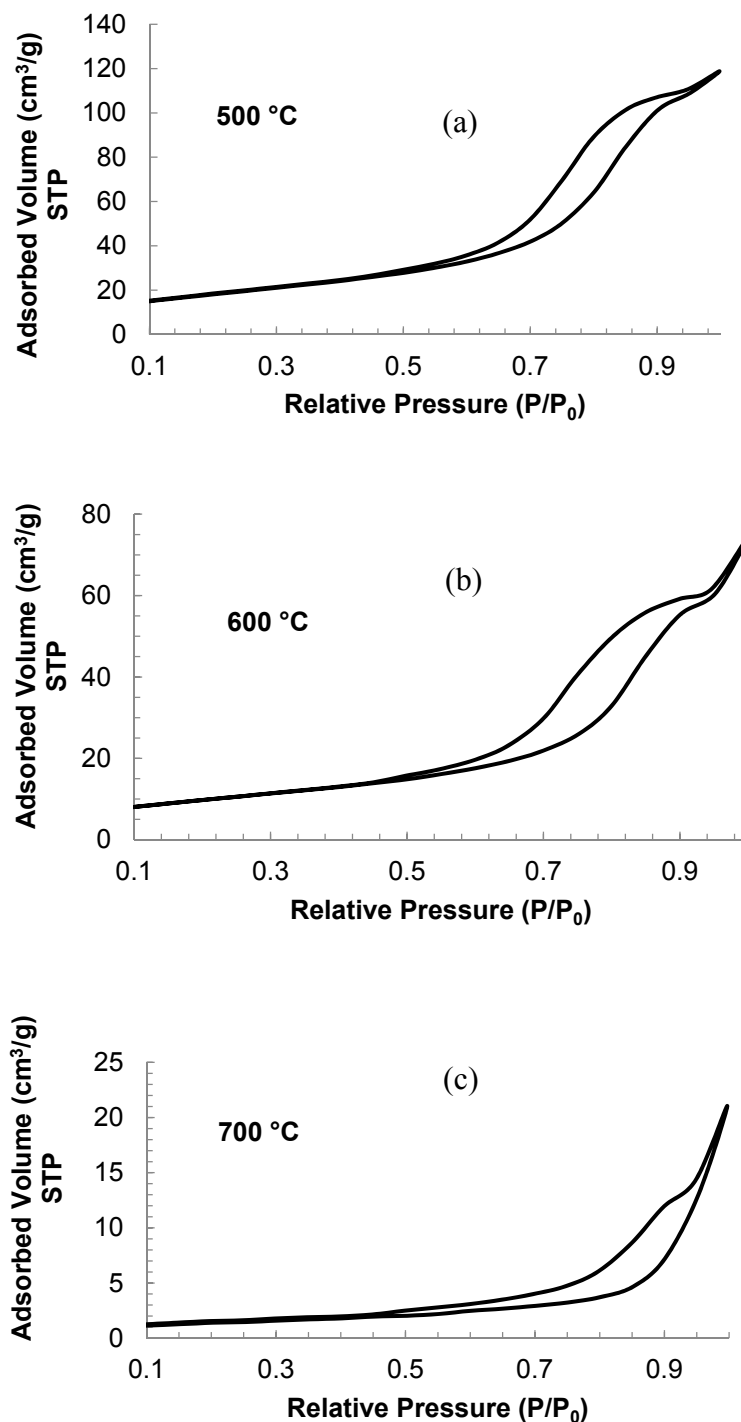


**Figure 4.** Adsorption isotherms for material calcined at different temperatures. (a) 500 °C; (b) 600 °C; (c) 700 °C.

The curves in Figure 4 indicate that the isotherms of the 500 and 600 °C samples are type V; whereas the isotherm for the sample calcined at 700 °C is more similar to a type III [34]. As mentioned above, this is a consequence of the pore diameter of the solid. On the other hand, it can be observed

that the adsorbed volume is larger for the sample calcined at 500 °C, which is congruent with the specific surface area estimated by the Brunauer, Emmet, and Teller (BET) method (Table 3).

The thermogravimetric analysis (Figure 5) was carried out to analyze the effect of the temperature on the chemical stability of the material after the programmed heating of the samples without calcining.

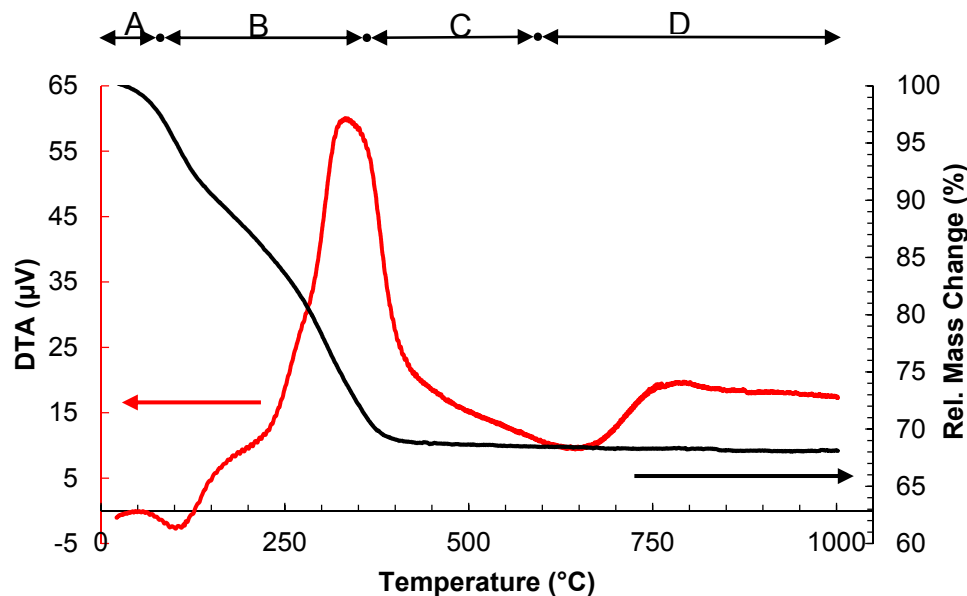


Figure 5. Differential thermogravimetric analysis and thermogram for synthesized material.

From Figure 5, four different regions are well differentiated from the differential thermal analysis (DTA): (A) loss of adsorbed water molecules under 150 °C; (B) Elimination of the precursors (sec-butanol, tert-butoxide, and glacial acetic acid) and chemisorbed water from 150 to 400 °C; (C) Formation of TiO<sub>2</sub> crystals from 400 to 600 °C; and (D) Stable weight loss over 600 °C [35]. This outcome supports the results of the XRD analysis, where the peak of the rutile phase appeared at 700 °C as reported in the literature [36,37].

## 2.2. Degradation and Loss of Antibacterial Activity of Commercial Amoxicillin by TiO<sub>2</sub>/WO<sub>3</sub>-Assisted Solar Photocatalysis

The results of the experimental design for the amoxicillin degradation are shown in Table 4: The highest amoxicillin degradation was achieved with the sample calcined at 700 °C, an initial amoxicillin concentration of 100 ppm and a catalyst load of 0.10 g L<sup>-1</sup>.

Table 4. Amoxicillin solar photocatalytic degradation.

		Calcination Temperature, °C					
		500		600		700	
Catalyst load [g L <sup>-1</sup> ]		0.05	0.10	0.05	0.10	0.05	0.10
Amoxicillin concentration [ppm]	100	39.8	28.6	58.6	31.7	45.6	64.4
	200	4.7	16.7	17.6	46.0	12.0	17.0

### 2.2.1. Effect of the Calcination Temperature

The most relevant fact that can favor the degradation of amoxicillin is that with a calcination temperature above 650 °C the rutile phase appears, and the photocatalytic activity of the synthesized material increases. This fact was evidenced on the XRD of Figure 3, which shows a small peak next to the anatase main peak.

As discussed before, the ratio of anatase/rutile of the sample calcined at 700 °C was found to be 74/26, which is very similar to that reported for the commercial TiO<sub>2</sub> Aeroxide P25 (Evonik, Essen, Germany) [28]. Although the surface area of this sample was the lowest of the three materials tested (due to the TiO<sub>2</sub> sintering at higher temperatures), the larger pore diameter seems to compensate this significant drawback of the catalyst. The sample calcined at 600 °C showed quite good performance as well, which suggests that there must be an optimum of calcination temperature between 600 and 700 °C. Further experiments should be carried out to synthesize a material not only with adequate surface area and particle size but also with a good photoactivity due to the rutile phase presence.

Regarding the  $E_g$ , the sample calcined at 700 °C showed the lowest value and its photocatalytic performance was the best of the three samples tested. This result is congruent with the main objective of the TiO<sub>2</sub> modification, which is to reduce the bandgap energy and to improve the photocatalytic activity.

### 2.2.2. Effect of the Initial Amoxicillin Concentration

The higher initial concentrations of the substrate in any photocatalytic reaction negatively affect the catalyst performance, as has been reported in several works [16,22,28]. In this study, the same behavior was observed as well.

The higher concentrations of amoxicillin are detrimental to the photocatalytic degradation because of the reduction of the available active sites of the catalyst after the adsorption of the amoxicillin and other compounds to the TiO<sub>2</sub>/WO<sub>3</sub> surface. In the case of higher concentrations, the adsorbed molecules can inhibit the •OH radicals' generation and the degradation rate decreases as a logical consequence.

### 2.2.3. Effect of the Catalyst Load

The catalyst load can have a positive effect on the photocatalytic degradation; that means that the performance will increase with an increase of the catalyst load as can be observed from the results shown in Table 4.

Nonetheless, the presence of a maximum has been reported in previous studies [22,38–40], which is around 0.35 g L<sup>-1</sup> for a CPC reactor of the same characteristics used for this research but with TiO<sub>2</sub> P25 as the catalyst. The existence of this maximum is because of the “clouding” effect in the reactor when higher catalyst loads are used in photocatalytic reactions. This phenomenon occurs when an excessive number of particles suspended in the reactor does not allow the photon to pass through the bulk liquid, and therefore, it avoids the generation of the electron-hole pairs necessary for the •OH formation.

The highest catalyst load used in these experiments (0.10 g L<sup>-1</sup>) is still lower than the maximum mentioned above; consequently, it is expected that better degradations are achieved with this value. From Table 4, it can be observed that only the samples calcined at 700 °C show this behavior.

As mentioned above, the sample of 700 °C exhibited the largest crystal size and accordingly, the largest cluster size. With these characteristics, they exhibit less scattering and photon absorption due to their larger size and thus, higher catalyst loads are required to generate the same amount of •OH radicals than the solids with smaller sizes (samples calcined at 500 and 600 °C) [38–40].

Although the effect of the pH was not considered in this study since the experiments were carried out at the natural pH of the solution (6.8–7.0), it is reported that the particle size is affected by the pH [5]. When the solution pH is close to the zero-charge point (pH<sub>zpc</sub>) of the solid, this tends to form large clusters with the consequences mentioned above. For the commercial TiO<sub>2</sub>, the reported pH<sub>zpc</sub> is around 6.5 [41]; therefore, it is probable that the value for the synthesized material in this study is similar and large clusters are formed.

#### 2.2.4. Kinetic Analysis of the Amoxicillin Photocatalytic Degradation

The  $\text{TiO}_2/\text{WO}_3$  calcined at  $700\text{ }^\circ\text{C}$  was chosen for the comparative kinetic study of the solar photocatalytic degradation of commercial amoxicillin. Figure 6 shows a comparison between the performance of this catalyst and the Aeroxide P25; both tested at the following reaction conditions: 100 ppm of the initial concentration of amoxicillin,  $0.1\text{ g L}^{-1}$  for catalyst load and  $510,000\text{ J m}^{-2}$  of UVA (Ultraviolet A) accumulated radiation.

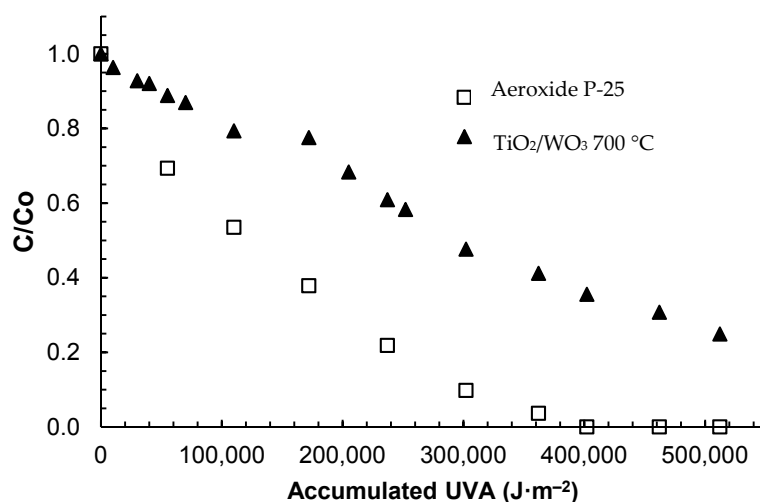


**Figure 6.** Photocatalytic degradation of amoxicillin with  $\text{TiO}_2/\text{WO}_3$  and Aeroxide P25.

The accumulated UVA energy was set as the independent variable instead of time because of the variability of the solar irradiation. Consequently, the kinetic law will be expressed in terms of the accumulated radiation that arrives at the solar reactor.

From Figure 6, it is evident that the P25 exhibited better performance than the  $\text{TiO}_2/\text{WO}_3$ . While the anatase/rutile ratio is very similar for both catalysts, the difference between the crystal sizes and the surface area are significant ( $50\text{ m}^2\text{ g}^{-1}$  for P25 vs.  $4.97\text{ m}^2\text{ g}^{-1}$  for  $\text{TiO}_2/\text{WO}_3$ ). The sintering of the  $\text{TiO}_2/\text{WO}_3$  particles at high calcination temperatures may be the primary cause of the formation of large clusters, as discussed previously.

On the other hand, the  $E_g$  of the  $\text{TiO}_2/\text{WO}_3$  is lower than the one of the P25; therefore, it was expected to have a higher photocatalytic degradation rate for the modified material since it could absorb photons of the visible part of the solar radiation spectrum.

Nonetheless, a lower  $E_g$  was not enough to improve the material performance over the P25 regarding photocatalytic applications. This result suggests that the modification of a semiconductor should not only be focused on decreasing the bandgap energy, but also on improving other properties that can affect the photocatalytic performance such as the surface area, pore diameter or the presence of photoactive crystalline phases significantly.

For analyzing the kinetics of the photocatalytic degradation, a modified Langmuir-Hinshelwood (L-H) was used and after fitting the model parameters. The obtained results are shown as follows in Table 5:

**Table 5.** Apparent kinetic and adsorption parameters of the modified L-H model.

Catalyst	$K_{\text{ads}}\ (\text{ppm}^{-1})$	$k_{\text{app}}\ (\text{ppm m}^2\ \text{J}^{-1})$
$\text{TiO}_2/\text{WO}_3$	0.0632	$1.88 \times 10^{-4}$
Aeroxide P25	0.0087	$1.14 \times 10^{-3}$

Results shown in Table 5 can be related to the difference between the specific surface area of the catalysts. Where the  $\text{TiO}_2/\text{WO}_3$  showed a higher value of the adsorption constant than the P25, the latter exhibited a higher apparent kinetic constant. The global reaction rate is limited by the kinetic for the case of the  $\text{TiO}_2/\text{WO}_3$  catalyst because of the surface can be covered easily by the substrates (that means a zero-order rate law). Whereas, for the P25, the behavior of the degradation kinetics fits a pseudo-first order law trend, where the adsorption can limit the rate or the kinetics indistinctly [41].

### 2.2.5. Loss of Antibiotic Power

Figure 7 shows a typical antibiogram, corresponding to the sample obtained at the most favorable conditions for the photocatalytic degradation of amoxicillin. This result suggests that the photo-oxidized amoxicillin could be transformed into a compound with less antibiotic activity.

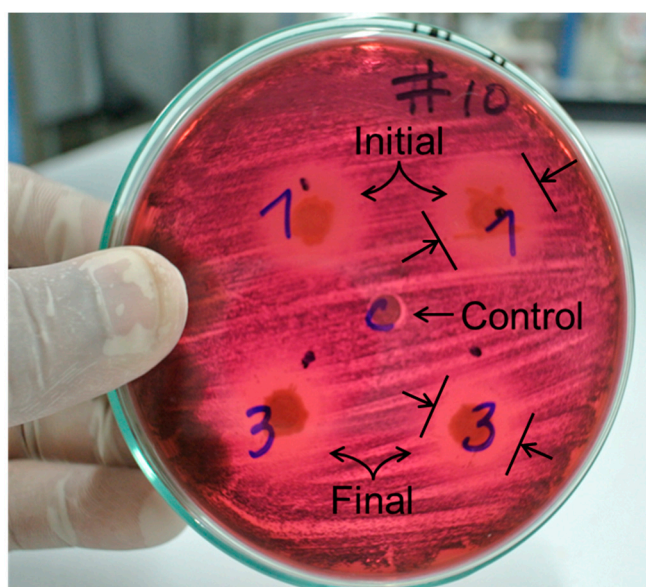


**Figure 7.** Antibiogram; (1) and (3) correspond to initial, and final simple for a treatment, (C) is a control.

It has been reported that the photocatalytic degradation of several pharmaceuticals can lead to more toxic byproducts [11,13,16,17]. Concerning antibiotics, the disappearance of the parent compound does not guarantee that the byproducts do not present antibacterial activity, despite the non-selective nature of the photocatalytic oxidation.

In Figure 7, the inhibition halo for the sample after photocatalytic treatment (3) is smaller than that observed for the sample before the treatment (1). From this observation, it can be proposed that the photocatalytic degradation yielded a lower number of antibiotic byproducts. This outcome is congruent with previous works that used  $\text{TiO}_2$ -assisted photocatalysis for removing amoxicillin and other antibiotics [11–13,16,17]. This result can be used in future works that study the coupling of heterogeneous solar photocatalysis to a biological system to polish the wastewater treatment.

## 3. Materials and Methods

### 3.1. Preparation of $\text{TiO}_2/\text{WO}_3$ Catalysts

For synthesizing  $\text{TiO}_2/\text{WO}_3$ , ammonium p-tungstate (ApT) (Sigma-Aldrich, Cali, Colombia), tetrabutyl orthotitanate (TBT) (Fluka, Bogota, Colombia), sec-butanol (SB) (Thermo Fisher Scientific, Bogota, Colombia), and glacial acetic acid (GAA) (Sigma-Aldrich, Cali, Colombia) were used. For dilutions, ultrapure water (MilliQ) with an  $18 \text{ M}\Omega \text{ cm}^{-1}$  resistivity (Merck, Cali, Colombia) was used.

The catalyst was prepared by using the sol-gel process, as suggested in the previous studies of Ramos-Delgado et al. [8,9]. For obtaining 10 g of catalyst, 29.1 mL of TBT in 100 mL of SB were mixed. The pH was adjusted to 3.5 GAA units. The pre-hydrolytic treatment was carried out with a mixture of 56.3 mL of SB and 1.15 mL of H<sub>2</sub>O. Then, the ApT solution (89 mg ApT in 7.5 mL of water) was slowly added dropwise. Finally, the solution was aged for two days; the resulting powder was finely macerated in an agate mortar before calcination. Moreover, three temperature calcination of the material 500, 600 and 700 °C were evaluated.

### 3.2. Photocatalyst Characterization

A UV-Vis spectrophotometer with diffuse reflectance analyzed the optical absorption of the catalyst (Thermo Fisher Scientific Evolution 300 with integrating sphere, Bogota, Colombia) and used a sample of Spectralon as standard blank. The XRD spectra were obtained with a Siemens D500 XRD equipment (Bogota, Colombia). The crystal size and the crystalline phases present in each of the catalysts were determined by using the Gsas© and Xpert© software packages; while the surface and pore diameter areas and adsorption isotherms were determined with a Quantachrome Autosorb Automated Gas Sorption equipment. Simultaneously, a thermogravimetry analysis (DTA/TG) was performed on a Simultaneous Thermal Analysis (STA) equipment PT1600 TG-DSC/DTA (LINSEIS, Monterrey, Mexico) to determine the behavior of the material in terms of thermal decomposition and phase changes.

### 3.3. Evaluation of the Photocatalytic Performance

A multilevel factorial experiment design was used for evaluating the following factors: the concentration of catalyst (0.10 g L<sup>-1</sup> and 0.05 g L<sup>-1</sup>), the concentration of amoxicillin (100 and 200 ppm), and the calcination temperature (500, 600 and 700 °C). The selected response variable was the degradation of amoxicillin [26,42]. The photocatalytic reaction was carried out in a CPC reactor with 25 L of total volume (Figure 8). The UV accumulated radiation was measured with a UV-radiometer Delta OHM HD210.2 (Bogota, Colombia). For each test, the accumulated energy was fixed at 550,000 J m<sup>-2</sup>. The commercial amoxicillin for the experimental runs was used as received from 500 mg-capsules (Genfar, Bogota, Colombia). For following the amoxicillin concentration, UPLC analyses were performed using an ACQUITY UPLC BEH<sup>®</sup> C18 1.7 μm column H-Class (Waters, Bogota, Colombia), with a retention time of 1.36 min. The experimental procedure for carrying out the solar photocatalytic tests was previously reported by Colina-Márquez et al. [41].



**Figure 8.** Solar pilot-scale CPC reactor (Photocatalysis lab, Universidad del Valle, Cali, Colombia).

### 3.4. Kinetic Analysis

The Langmuir-Hinshelwood expression was modified to consider the change of the amoxicillin concentrations with respect to the accumulated UVA radiation, as follows:

$$\frac{dC}{dQ_{UV}} = \frac{k_{app}K_{Ads}C}{1 + K_{Ads}C} \quad (3)$$

where C is the amoxicillin concentration in ppm,  $K_{Ads}$  is the adsorption constant in  $\text{ppm}^{-1}$ ,  $Q_{UV}$  is the accumulated UVA radiation in  $\text{J m}^{-2}$  and  $k_{app}$  is the apparent kinetic constant in  $\text{ppm} \cdot \text{m}^2 \text{J}^{-1}$ . For estimating the model parameters, Equation (3) is transformed into its linear form for fitting its parameters from the experimental data by using linear regression:

$$\frac{dQ_{UV}}{dC} = \frac{1}{k_{app}K_{Ads}} \cdot \frac{1}{C} + \frac{1}{k_{app}} \quad (4)$$

The reciprocal of the term  $dC/dQ_{UV}$ , which is analog to  $dC/dt$ , was plotted versus the reciprocal of the concentration ( $1/C$ ). By using the minimum squares analysis, the model parameters,  $K_{Ads}$  and  $k_{app}$ , were estimated from the slope and the y-intercept of the curve fitted to the experimental results.

### 3.5. Determination of Inhibition Halo

An antibiogram was performed for determining the potential loss of antibiotic power of the amoxicillin [43]. The reactants used for this test were: eosin Methylene Blue agar (Lot. VM290047 124, Merck, Cali, Colombia), nutrient agar (Lot. 16761, Bogota, Colombia), Bacto™ Peptone (Lot. 3063372, Becton Dickinson, Bogota, Colombia) and E. Coli. (WG5) as the model bacterium. The tests were carried out in Petri's boxes of 9 cm and an incubator (WTB Binder, Tuttlingen, Germany) with a McFarland 0.5 standard for determining the concentration of colonies forming units (CFU) of present bacteria.

## 4. Conclusions

The calcination temperature had a significant effect on the photocatalytic performance for removing amoxicillin. The material synthesized at 700 °C was the only one that exhibited the presence of the rutile crystalline phase in its structure. Nonetheless, it underperformed compared with the commercial standard, Aeroxide P25, which could remove all the amoxicillin with less UVA accumulated radiation than the required one by the  $\text{TiO}_2/\text{WO}_3$  catalyst. Regarding the loss of antibacterial activity, the inhibition test showed that  $\text{TiO}_2/\text{WO}_3$ -assisted photocatalytic degradation yields oxidation byproducts with less antibiotic activity than the original amoxicillin.

**Author Contributions:** A.A.-S. carried out the synthesis and the evaluation experiments with solar photocatalysis; F.M.-M. gave the support of his lab for the experimental tests; C.B.-L. helped to structure and write this paper; A.H.-R. provided the support for characterizing the catalysts, and J.C.-M. analyzed and processed the photocatalytic degradation results.

**Acknowledgments:** The financial and logistic support of Universidad del Valle, Universidad de Cartagena, Universidad Autónoma de Nuevo León, and Ryerson University for their financial and logistic support. A.A. would like to thank Colciencias for his Ph.D. scholarship and J.C.-M. want to thank the Research Office at Universidad de Cartagena for Supporting Recognized Research Groups.

**Conflicts of Interest:** The authors declare no conflicts of interest.

## References

1. Fujishima, A.; Zhang, X.; Tryk, D. Heterogeneous photocatalysis: From water photolysis to applications in environmental cleanup. *Int. J. Hydrogen Energy* **2007**, *32*, 2664–2672. [[CrossRef](#)]
2. Alarcon, D.C.; Maldonado, M.I.; Malato, S.; Gernjak, W. Photocatalytic decontamination and disinfection of water with solar collectors. *Catal. Today* **2007**, *122*, 137–149.

3. Domènech, X.; Jardim, W.F.; Litter, M.I. Procesos avanzados de oxidación para la eliminación de contaminantes. In *Eliminación de contaminantes por fotocatalisis heterogénea*; Blesa, M.A., Ed.; CYTED: La Plata, Argentina, 2001; pp. 3–26.
4. Klavarioti, M.; Mantzavinos, D.; Kassinos, D. Removal of residual pharmaceuticals from aqueous systems by advanced oxidation processes. *Environ. Int.* **2009**, *35*, 402–417. [[CrossRef](#)] [[PubMed](#)]
5. Malato, S.; Fernández-Ibáñez, P.; Maldonado, M.I.; Blanco, J.; Gernjak, W. Decontamination and disinfection of water by solar photocatalysis: Recent overview and trends. *Catal. Today* **2009**, *147*, 1–59. [[CrossRef](#)]
6. Zaleska, A. Doped-TiO<sub>2</sub>: A Review. *Recent Patents Eng.* **2008**, *2*, 157–164. [[CrossRef](#)]
7. Shen, S.H.; Wu, T.Y.; Juan, J.C.; Teh, C.Y. Recent developments of metal oxide semiconductors as photocatalysts in advanced oxidation processes (AOPs) for treatment of dye waste-water. *J. Chem. Technol. Biotechnol.* **2011**, *86*, 1130–1158.
8. Ramos-Delgado, N.A.; Hinojosa-Reyes, L.; Guzman-Mar, J.L.; Gracia-Pinilla, M.A.; Hernández-Ramírez, A. Synthesis by sol–gel of WO<sub>3</sub>/TiO<sub>2</sub> for solar photocatalytic degradation of malathion pesticide. *Catal. Today* **2013**, *209*, 35–40. [[CrossRef](#)]
9. Ramos-Delgado, N.A.; Gracia-Pinilla, M.A.; Maya-Treviño, L.; Hinojosa-Reyes, L.; Guzman-Mar, J.L.; Hernández-Ramírez, A. Solar photocatalytic activity of TiO<sub>2</sub> modified with WO<sub>3</sub> on the degradation of an organophosphorus pesticide. *J. Hazard. Mater.* **2013**, *263*, 36–44. [[CrossRef](#)] [[PubMed](#)]
10. Yang, J.; Zhang, X.; Liu, H.; Wang, C.; Liu, S.; Sun, P.; Wang, L.; Liu, Y. Heterostructured TiO<sub>2</sub>/WO<sub>3</sub> porous microspheres: Preparation, characterization and photocatalytic properties. *Catal. Today* **2013**, *201*, 195–202. [[CrossRef](#)]
11. Elmolla, E.S.; Chaudhuri, M. Photocatalytic degradation of amoxicillin, ampicillin and cloxacillin antibiotics in aqueous solution using UV/TiO<sub>2</sub> and UV/H<sub>2</sub>O<sub>2</sub>/TiO<sub>2</sub> photocatalysis. *Desalination* **2010**, *252*, 46–52. [[CrossRef](#)]
12. Das, R.; Sarkar, S.; Chakraborty, S.; Choi, H.; Bhattacharjee, C. Remediation of Antiseptic Components in Wastewater by Photocatalysis Using TiO<sub>2</sub> Nanoparticles. *Ind. Eng. Chem. Res.* **2014**, *53*, 3012–3020. [[CrossRef](#)]
13. Fatta-Kassinos, D.; Vasquez, M.I.; Kümmerer, K. Transformation products of pharmaceuticals in surface waters and wastewater formed during photolysis and advanced oxidation processes—Degradation, elucidation of byproducts and assessment of their biological potency. *Chemosphere* **2011**, *85*, 693–709. [[CrossRef](#)] [[PubMed](#)]
14. Basile, T.; Petrella, A.; Petrella, M.; Boghetich, G.; Petruzzelli, V.; Colasuonno, S.; Petruzzelli, D. Review of Endocrine-Disrupting-Compound Removal Technologies in Water and Wastewater Treatment Plants: An EU Perspective. *Ind. Eng. Chem. Res.* **2011**, *50*, 8389–8401. [[CrossRef](#)]
15. Klauson, D.; Babkina, J.; Stepanova, K.; Krichevskaya, M.; Prei, S. Aqueous photocatalytic oxidation of amoxicillin. *Catal. Today* **2010**, *151*, 39–45. [[CrossRef](#)]
16. Chaudhuri, M.; Wahap, M.Z.B.A.; Affam, A.C. Treatment of aqueous solution of antibiotics amoxicillin and cloxacillin by modified photo-Fenton process. *Desalin. Water Treat.* **2013**, *51*, 7255–7268. [[CrossRef](#)]
17. Dimitrakopoulou, D.; Rethemiotaki, I.; Frontistis, Z.; Xekoukoulotakis, N.P.; Venieri, D.; Mantzavinos, D. Degradation, mineralization and antibiotic inactivation of amoxicillin by UV-A/TiO<sub>2</sub> photocatalysis. *J. Environ. Manag.* **2012**, *98*, 168–174. [[CrossRef](#)] [[PubMed](#)]
18. Frontistis, Z.; Antonopoulou, M.; Venieri, D.; Konstantinou, I.; Mantzavinos, D. Boron-doped diamond oxidation of amoxicillin pharmaceutical formulation: Statistical evaluation of operating parameters, reaction pathways and antibacterial activity. *J. Environ. Manag.* **2017**, *195*, 100–109. [[CrossRef](#)] [[PubMed](#)]
19. Chen, X. Increasing Solar Absorption for Photocatalysis with Black Hydrogenated Titanium Dioxide Nanocrystals. *Science* **2013**, *331*, 746–750. [[CrossRef](#)] [[PubMed](#)]
20. Li, X.Z.; Li, F.B.; Yang, C.L.; Ge, W.K. Photocatalytic activity of WO<sub>x</sub>-TiO<sub>2</sub> under visible light irradiation. *J. Photochem. Photobiol. A Chem.* **2001**, *141*, 209–217. [[CrossRef](#)]
21. Mccullagh, C.; Skillen, N.; Adams, M.; Robertson, P.K.J. Photocatalytic reactors for environmental remediation: A review. *J. Chem. Technol. Biotechnol.* **2011**, *86*, 1002–1017. [[CrossRef](#)]
22. Colina-Márquez, J.; Díaz, D.; Rendón, A.; López-Vásquez, A.; Machuca-Martínez, F. Photocatalytic treatment of a dye polluted industrial effluent with a solar pilot-scale CPC reactor. *J. Adv. Oxid. Technol.* **2009**, *12*, 93–99. [[CrossRef](#)]
23. Xiaobo, C. Titanium Dioxide Nanomaterials and Their Energy Applications. *Chin. J. Catal.* **2009**, *30*, 839–851.

24. Liu, K.; Hsueh, Y.; Su, C.; Perng, T. Photoelectrochemical application of mesoporous TiO<sub>2</sub>/WO<sub>3</sub> nanohoneycomb prepared by sol e gel method. *Int. J. Hydrogen Energy* **2013**, *38*, 7750–7755. [[CrossRef](#)]
25. Piszcz, M.; Tryba, B.; Grzmił, B.; Morawski, A.W. Photocatalytic Removal of Phenol Under UV Irradiation on WOX–TiO<sub>2</sub> Prepared by Sol – Gel Method. *Catal. Lett.* **2009**, *128*, 190–196. [[CrossRef](#)]
26. Weng, X.; Chen, Z.; Chen, Z.; Megharaj, M. Colloids and Surfaces A: Physicochemical and Engineering Aspects Clay supported bimetallic Fe/Ni nanoparticles used for reductive degradation of amoxicillin in aqueous solution: Characterization and kinetics. *Colloids Surf. A Physicochem. Eng. Asp.* **2014**, *443*, 404–409. [[CrossRef](#)]
27. Haider, A.J.; Anbari, R.H.A.; Kadhim, G.R.; Salame, C.T. Exploring potential Environmental applications of TiO<sub>2</sub> Nanoparticles. *Energy Procedia* **2017**, *119*, 332–345. [[CrossRef](#)]
28. Herrera-Barros, A.; Reyes, A.; Colina-Marquez, J. Evaluation of the photocatalytic activity of iron oxide nanoparticles functionalized with titanium dioxide. *J. Phys. Conf. Ser.* **2016**, *687*, 012034. [[CrossRef](#)]
29. Yu, J.-G.; Yu, H.-G.; Cheng, B.; Zhao, X.-J.; Yu, J.C.; Ho, W.-K. The Effect of Calcination Temperature on the Surface Microstructure and Photocatalytic Activity of TiO<sub>2</sub> Thin Films Prepared by Liquid Phase Deposition. *J. Phys. Chem. B* **2003**, *107*, 13871–13879. [[CrossRef](#)]
30. Escobedo-Morales, A.; Sánchez-Mora, E.; Pal, U. Use of diffuse reflectance spectroscopy for optical characterization of un-supported nanostructures. *Rev. Mex. Fís.* **2007**, *53*, 18–22.
31. Beranek, R.; Kisch, H. Tuning the optical and photoelectrochemical properties of surface-modified TiO<sub>2</sub>. *Photochem. Photobiol. Sci.* **2008**, *7*, 40–48. [[CrossRef](#)] [[PubMed](#)]
32. Patsoura, A.; Kondarides, D.I.; Verykios, X.E. Enhancement of photoinduced hydrogen production from irradiated Pt/TiO<sub>2</sub> suspensions with simultaneous degradation of azo-dyes. *Appl. Catal. B Environ.* **2006**, *64*, 171–179. [[CrossRef](#)]
33. Bezrodna, T.; Gavrilko, T.; Puchkovska, G.; Shimanovska, V.; Baran, J. Spectroscopic study of TiO<sub>2</sub> (rutile) –benzophenone heterogeneous systems. *J. Mol. Struct.* **2002**, *614*, 315–324. [[CrossRef](#)]
34. Enríquez, J.M.H.; Serrano, L.A.G.; Soares, B.H.Z.; Alamilla, R.G.; Resendiz, B.B.Z.; Del Sánchez, T.; Hernández, A.C. Síntesis y Caracterización de Nanopartículas de N-TiO<sub>2</sub> – Anatasa. *Superf. y Vacío* **2008**, *21*, 1–5.
35. Rungjaroentawon, N.; Onsuratoom, S.; Chavadej, S. Hydrogen production from water splitting under visible light irradiation using sensitized mesoporous-assembled TiO<sub>2</sub>-SiO<sub>2</sub> mixed oxide photocatalysts. *Int. J. Hydrogen Energy* **2012**, *37*, 11061–11071. [[CrossRef](#)]
36. Yang, H.; Shi, R.; Zhang, K.; Hu, Y.; Tang, A.; Li, X. Synthesis of WO<sub>3</sub>/TiO<sub>2</sub> nanocomposites via sol-gel method. *J. Alloys Compd.* **2005**, *398*, 200–202. [[CrossRef](#)]
37. Djaoued, Y.; Badilescu, S.; Ashrit, P.V.; Bersani, D.; Lottici, P.; Robichaud, J. Study of Anatase to Rutile Phase Transition in Nanocrystalline Titania Films. *J. Sol-Gel Sci. Technol.* **2002**, *24*, 255–264. [[CrossRef](#)]
38. Colina-Márquez, J.; Machuca, F.; Puma, G.L. Radiation Absorption and Optimization of Solar Photocatalytic Reactors for Environmental Applications. *Environ. Sci. Technol.* **2010**, *44*, 5112–5120. [[CrossRef](#)] [[PubMed](#)]
39. Mueses, M.A.; Machuca-Martinez, F.; Hernández-Ramirez, A.; Puma, G.L. Effective radiation field model to scattering—Absorption applied in heterogeneous photocatalytic reactors. *Chem. Eng. J.* **2015**, *279*, 442–451. [[CrossRef](#)]
40. Nasirian, M.; Lin, Y.P.; Bustillo-Lecompte, C.F.; Mehrvar, M. Enhancement of photocatalytic activity of titanium dioxide using non-metal doping methods under visible light: A review. *Int. J. Environ. Sci. Technol.* **2017**, 1–24. [[CrossRef](#)]
41. Colina-Márquez, J.; Machuca-Martínez, F.; Puma, G.L. Photocatalytic mineralization of commercial herbicides in a pilot-scale solar CPC reactor: Photoreactor modeling and reaction kinetics constants independent of radiation field. *Environ. Sci. Technol.* **2009**, *43*, 8953–8960. [[CrossRef](#)] [[PubMed](#)]
42. Xu, H.; Cooper, W.J.; Jung, J.; Song, W. Photosensitized degradation of amoxicillin in natural organic matter isolate solutions. *Water Res.* **2011**, *45*, 632–638. [[CrossRef](#)] [[PubMed](#)]
43. Cantón, R.; Gómez-Lus, M.L.; Rodríguez-Avial, C.; Martínez, L.M.; Vila, J. *Procedimientos en Microbiología Clínica*; SIEMC: Madrid, Spain, 2000; pp. 10–20.

